

AUTOMATED DISCOVERY OF PARSIMONIOUS SPECTRAL INDICES VIA NORMALIZED DIFFERENCE POLYNOMIALS

ALI LOTFI¹, ADAM CARTER², THUAN HA¹, MOHAMMAD MEYSAMI³, KWABENA NKETIA¹, STEVE SHIRTLIFFE¹

¹Nutrien Centre for Sustainable and Digital Agriculture, Department of Plant Sciences, University of Saskatchewan, Saskatoon, SK, Canada

²Crop Development Centre, Department of Plant Sciences, University of Saskatchewan, Saskatoon, SK, Canada

³Department of Economics, Applied Statistics, and International Business, New Mexico State University, Las Cruces, NM, USA

ABSTRACT. We introduce an automated way to find compact spectral indices for vegetation classification. The idea is to take all pairwise normalized differences from the spectral bands and then build polynomial combinations up to a fixed degree, which gives a structured search space that still keeps the illumination invariance needed in remote sensing. For a sensor with n bands this produces $\binom{n}{2}$ base normalized differences, and the degree-2 polynomial expansion gives 1,080 candidate features for the 10-band Sentinel-2 configuration we use here. Feature selection methods (ANOVA filtering, recursive elimination, and L_1 -regularized SVM) then pick out small sets of indices that reach the desired accuracy, so the final models stay simple and easy to interpret. We test the framework on Kochia (*Bassia scoparia*) detection using Sentinel-2 imagery from Saskatchewan, Canada ($N = 2,318$ samples, 2022–2024). A single degree-2 index, the product of two normalized differences from the red-edge bands, already reaches 96.26% accuracy, and using eight indices only raises this to 97.70%. In every case the chosen features are degree-2 products built from bands b_4 through b_8 , which suggests that the discriminative signal comes from spectral *interactions* rather than individual band ratios. Because the indices involve only simple arithmetic, they can be deployed directly in platforms like Google Earth Engine. The same approach works for other sensors and classification tasks, and an open-source implementation (`ndindex`) is available.

INTRODUCTION

Remote sensing has transformed how we monitor vegetation in agricultural areas. It allows us to observe large regions consistently, which would be difficult to do with field surveys alone [34]. Among the tools for working with multispectral imagery, normalized difference indices are especially valuable because they are simple to calculate and have a clear physical meaning [1]. A normalized difference index is found by taking the difference between two spectral bands and dividing it by their sum. This straightforward ratio offers several practical benefits for agriculture: it remains stable under changes in lighting, is less affected by topographic shading, and is more reliable across different sensor calibrations [1].

The Normalized Difference Vegetation Index (NDVI) was first introduced by Rouse et al. (1973) at Texas A&M University during the Great Plains Corridor Project and it soon became a classic example of a simple normalized index [32]. The index was created to deal with the confusing effects of changing solar zenith angle on satellite observations taken along different latitudes. NDVI makes use of the characteristic spectral behavior of photosynthetically active vegetation, where chlorophyll absorbs most of the red light while plant cells reflect strongly in the near infrared region [32]. When the difference between near infrared (NIR) and red reflectances is written in normalized form, NDVI tends to reduce atmospheric effects and gives a fairly stable measure of vegetation greenness. This single quantity has been shown to relate closely to important biophysical variables such as leaf area index (LAI), chlorophyll concentration and fractional vegetation cover [10].

The way band ratios and normalized differences are constructed tends to bring out the composition we care about while pushing down many confusing effects in the scene, for example terrain slope or changes in grain size [33]. This behavior has been very useful in precision agriculture, where farmers and researchers want indicators of crop health that they can trust and that stay roughly stable under different illumination, sun angles and atmospheric conditions [9]. Over time the NDVI literature has grown very fast. The number of NDVI related publications went from 795 in the 1990s to more than 12,618 in the 2010s, which shows how widely normalized indices are now used in agricultural and environmental monitoring work [29].

The success of NDVI has encouraged the creation of many other spectral indices, each one aimed at fixing certain limitations or making better use of particular spectral features. The Soil Adjusted Vegetation Index (SAVI), introduced by Huete (1988), adds a soil brightness term so that background soil reflectance has less influence in areas where vegetation is sparse [12]. The Enhanced Vegetation Index (EVI) goes a step further by using blue band reflectance to correct remaining atmospheric effects and to ease saturation in regions with very dense biomass [11]. In more recent years, the spread of sensors with red edge bands, especially the Sentinel 2 Multi Spectral Instrument (MSI), has led to indices such as the Normalized Difference Red Edge Index (NDRE), which are more sensitive to changes in chlorophyll content and plant nitrogen status [28].

These spectral indices are now widely used in crop classification and in agricultural monitoring. Sonobe et al. (2018) showed that 82 published vegetation indices computed from Sentinel 2 MSI data can support crop type classification when they are used in ensemble learning approaches [28]. The red edge bands that are specific to Sentinel 2, sitting between the red and near infrared parts of the spectrum, work especially well for picking up small changes in crop canopy traits and for separating vegetation species at fairly fine taxonomic levels [13, 14]. In the same line, more recent studies report that the Sentinel 2 spectral configuration allows reliable weed detection in maize fields, with user and producer accuracies above 88%, which shows that the sensor is quite sensitive to biophysical differences between the crop and invasive species [22].

Despite these advances in general weed detection, some invasive species remain difficult to identify. For Kochia (*Bassia scoparia*), spotting the plants reliably in remote sensing images is still a bit of a challenge. In many fields they share a lot of morphological and spectral traits with the

surrounding crops, so the signals get mixed. Work with hyperspectral imagery has reported classification accuracies of 67–80% for separating herbicide resistant Kochia biotypes using support vector machine classifiers [24, 27]. More recent studies have tried attention based convolutional neural networks and have pushed the accuracy above 99% when separating Kochia from sugarbeet under field conditions [20]. These approaches are powerful, but they usually depend on costly hyperspectral sensors and fairly involved computational setups, which makes them awkward to use for everyday regional monitoring.

Deep learning methods often give very strong classification results in remote sensing, but using them in everyday agricultural systems is still tricky because they are hard to interpret. A typical deep neural network behaves like a black box, so it is difficult to see why the model prefers one class over another [25, 26]. In earth observation work many practitioners want more than good accuracy, they also want ecological insight and some sense of the processes behind the signal, and this lack of transparency gets in the way of that goal [19].

Opacity in complex machine learning models creates problems that go beyond simple curiosity about how they work. In agricultural decisions, people on the ground and in offices farmers, agronomists and policy makers need to know why a model suggests a certain action before they are willing to follow it [23]. When models are built from polynomial functions of familiar spectral indices, the link to biophysical processes is much clearer, so experts can check whether the model behavior agrees with established scientific knowledge [3]. By contrast, many deep learning models, though very good at capturing intricate patterns in the spectral and spatial domain, still behave largely as black boxes and make it hard to interpret the ecological processes behind their predictions [18].

In contrast, smaller models built from interpretable spectral features have several very practical advantages. They usually handle shifts between training and deployment data better, they need fewer computational resources at prediction time, and they can be run on many different remote sensing platforms without any special hardware [5]. The basic idea of parsimony is that, when two models give roughly the same predictive performance, the simpler one is usually the better choice, since it is less likely to overfit and more likely to work well on new data [16].

The design of new spectral indices has mostly depended on expert judgment, physical intuition, and a good amount of trial and error. In practice, researchers usually write down candidate formulas from their understanding of spectral responses and then test them against ground truth measurements to see how well they behave [2, 31]. This style of empirical tuning takes a lot of time and effort, and it can still lead to solutions that are not very close to optimal. Because there are so many ways to combine bands, apply transformations, and choose coefficients, checking every possibility by hand is essentially impossible except for the very simplest index forms.

Even a fairly modest multispectral sensor with ten spectral bands already gives a surprising number of choices. One can form 45 distinct normalized differences from all possible pairs of bands, around 120 different three band combinations once adjustment terms are included, and then many more formulas built from products, powers, or ratios inside other ratios. When extra sensor capabilities are added, for example the 13 bands on Sentinel 2 MSI, the space of candidate indices quickly becomes enormous [21]. In practice this means that many useful index formulas

are probably still unknown, because most studies stay close to a few familiar indices and only try variations that match existing physical intuition.

Choosing an index is also very context dependent. It depends on the task, the species of interest, the sensor, and even the local conditions in the field. An index that works nicely for detecting crop stress can still be poor at telling weeds from the crop, and a formula tuned for one sensor may not carry over to another one unless it is recalibrated. Because of this, it makes sense to look for more automatic, data driven ways to search for indices. Such approaches could speed up the design of indices tailored to particular applications and at the same time reveal useful new formulations that experts might not think of on their own.

These considerations, the demonstrated value of normalized differences, the need for interpretable models, and the limits of manual index design—motivate automated methods for discovering parsimonious spectral formulations. The goal is to identify small feature sets that obtain high classification accuracy while being simple and interpretable enough for operational deployment.

Genetic programming and related evolutionary search methods offer another way to design indices automatically in remote sensing work. Olague and co workers showed that spectral indices can be evolved with genetic programming for soil erosion studies, and Makkeasorn et al. (2009) used a two stage genetic programming scheme to choose vegetation indices for riparian zone monitoring [17]. More recently, Hernández-Clemente et al. (2022) applied genetic programming to detect plant infestations from multispectral aerial imagery and reported classification accuracies above 96%. Across these studies, the common benefit is that genetic programming can explore very large spaces of possible formulas while still tending to keep indices fairly simple when the fitness function is set up with parsimony in mind.

Feature selection tools from machine learning provide another way to find small but effective sets of features inside rich spectral data. Common options include filter methods (for example ANOVA based SelectKBest), wrapper methods (such as recursive feature elimination), and embedded methods (for example L1 regularized support vector machines), each with its own way of trading off classification accuracy against model complexity [7]. When these ideas are applied to spectral indices derived from satellite imagery, they can be used to pick out the indices that really carry most of the information for a particular classification task.

In this study we introduce a simple framework for finding compact spectral indices that work well for vegetation classification using Sentinel 2 satellite imagery. We build a feature space for the satellite data by taking normalized difference indices and forming polynomial features of a fixed degree. In practice we only consider polynomials of degree at most two in the normalized difference basis, so we end up with three kinds of features: linear terms $ND(i) = (b_i - b_j)/(b_i + b_j)$, squared terms $(ND(i))^2$, and interaction terms $ND(i) \cdot ND(k)$. This fixed degree polynomial construction keeps the usual illumination invariance of normalized differences but still lets us capture useful nonlinear spectral relationships.

We use three complementary feature selection algorithms: SelectKBest with ANOVA F statistics, recursive feature elimination (RFE), and L1 regularized support vector machines. Together they allow us to choose small subsets of features from the polynomial embedding that still give

strong classification accuracy. We illustrate the approach on Kochia (*Bassia scoparia*) classification and find that simple affine combinations of the normalized difference polynomials can reach accuracies above 97% using only four spectral features. Although the examples in this paper focus on Kochia detection, the same procedure is general and can be applied to other crop and weed classification tasks, because the polynomial embedding and feature selection steps do not depend on the particular species. The indices produced in this way keep the mathematical structure needed for physical interpretation, while remaining simpler than many existing alternatives and easy to use on different sensor platforms.

1. NORMALIZED DIFFERENCE POLYNOMIAL FRAMEWORK

Consider a multispectral sensor providing n spectral channels with reflectance values b_1, b_2, \dots, b_n , where each $b_i \geq 0$ represents the measured reflectance in the i -th spectral band.

Definition 1.1 (Normalized Difference). For any pair of spectral bands b_i and b_j with $i \neq j$, the *normalized difference* is defined as:

$$(1.1) \quad \text{ND}_{ij} = \frac{b_i - b_j}{b_i + b_j + \varepsilon}$$

where $\varepsilon > 0$ is a small regularization constant (typically $\varepsilon = 10^{-10}$) that ensures numerical stability for all non-negative reflectance values, including edge cases where $b_i + b_j \approx 0$.

The normalized difference formulation possesses several properties that make it particularly suitable for remote sensing applications. First, ND_{ij} is invariant to multiplicative scaling of the input bands: if $(b_i, b_j) \mapsto (\alpha b_i, \alpha b_j)$ for any $\alpha > 0$, then ND_{ij} remains practically unchanged. This property confers robustness to variations in solar illumination intensity, atmospheric transmittance, and sensor gain [33]. Second, the normalized difference is antisymmetric, satisfying $\text{ND}_{ji} = -\text{ND}_{ij}$, which implies that the set of distinct normalized differences has cardinality $\binom{n}{2}$.

For n spectral bands, the complete set of normalized differences is:

$$(1.2) \quad \mathcal{N} = \{\text{ND}_{ij} : 1 \leq i < j \leq n\}, \quad |\mathcal{N}| = \binom{n}{2}$$

We build a feature space made of polynomial functions in the normalized difference basis. By keeping the polynomial degree fixed we keep the model from becoming too complex, while still letting it describe useful nonlinear spectral patterns.

Definition 1.2 (Normalized Difference Polynomial of Degree d). A *normalized difference polynomial of degree d* is a function $p : \mathbb{R}^n \rightarrow \mathbb{R}$ of the form:

$$(1.3) \quad p(b_1, \dots, b_n) = \sum_{\mathbf{k}} c_{\mathbf{k}} \prod_{(i,j) \in \mathcal{N}} \text{ND}_{ij}^{k_{ij}}$$

where $\mathbf{k} = (k_{ij})_{(i,j) \in \mathcal{N}}$ ranges over multi-indices with $k_{ij} \in \mathbb{Z}_{\geq 0}$ satisfying $\sum_{(i,j)} k_{ij} \leq d$, and $c_{\mathbf{k}} \in \mathbb{R}$ are coefficients.

In this work, we focus on polynomials of degree at most two ($d \leq 2$). This choice balances expressiveness against interpretability: degree-2 terms capture pairwise interactions between spectral transitions, while higher degrees rapidly increase the feature space; degree-3 would give over 20,000 features for 10 bands. This trades interpretability for marginal gains. Empirically, degree-2 suffices for providing an index for Kochia. This yields three types of features:

Degree 1 (Linear terms): The normalized differences themselves:

$$(1.4) \quad \Phi^{(1)} = \{\text{ND}_{ij} : 1 \leq i < j \leq n\}, \quad |\Phi^{(1)}| = \binom{n}{2}$$

Degree 2 (Quadratic terms): Squares and products of normalized differences:

$$(1.5) \quad \Phi_{\text{sq}}^{(2)} = \{\text{ND}_{ij}^2 : 1 \leq i < j \leq n\}, \quad |\Phi_{\text{sq}}^{(2)}| = \binom{n}{2}$$

$$(1.6) \quad \Phi_{\text{prod}}^{(2)} = \{\text{ND}_{ij} \cdot \text{ND}_{kl} : (i, j) < (k, l)\}$$

where the ordering is lexicographic, and $|\Phi_{\text{prod}}^{(2)}| = \binom{\binom{n}{2}}{2}$. The complete degree-2 polynomial feature space is:

$$(1.7) \quad \Phi = \Phi^{(1)} \cup \Phi_{\text{sq}}^{(2)} \cup \Phi_{\text{prod}}^{(2)} \cup \{1\}$$

where $\{1\}$ represents the constant (intercept) term. The total number of features (excluding the intercept) is:

$$(1.8) \quad |\Phi| - 1 = \binom{n}{2} + \binom{n}{2} + \binom{\binom{n}{2}}{2} = 2\binom{n}{2} + \binom{\binom{n}{2}}{2}$$

Remark. For Sentinel-2 imagery using bands b_1 through b_{10} (excluding SWIR bands b_{11} and b_{12}), we have $n = 10$, yielding $\binom{10}{2} = 45$ normalized differences, 45 squared terms, and $\binom{45}{2} = 990$ product terms, for a total of $|\Phi| - 1 = 1080$ features.

A key advantage of the normalized difference polynomial framework is that the feature space is inherently bounded, enabling principled scaling of classifier outputs to interpretable ranges.

Proposition 1.3 (Boundedness of ND Polynomials). *Let $p(b_1, \dots, b_n)$ be a normalized difference polynomial of degree d with finitely many nonzero coefficients. Then:*

- (i) *Each normalized difference satisfies $\text{ND}_{ij} \in (-1, 1)$ for all $b_i, b_j \geq 0$.*
- (ii) *The polynomial p extends continuously to the closure $[-1, 1]^{|\mathcal{N}|}$. Let $M = \max_{(\text{ND}_{ij}) \in [-1, 1]^{|\mathcal{N}|}} |p|$ denote the maximum absolute value of p on the closed hypercube. Then $|p(\mathbf{b})| \leq M$ for all $\mathbf{b} \in \mathcal{D} = \{(b_1, \dots, b_n) : b_i \geq 0\}$.*
- (iii) *The scaled function $\tilde{p} = p/M$ satisfies $\tilde{p}(\mathbf{b}) \in [-1, 1]$ for all $\mathbf{b} \in \mathcal{D}$.*

Proof. (i) For $b_i, b_j \geq 0$, we have $|b_i - b_j| \leq b_i + b_j < b_i + b_j + \varepsilon$ (strict inequality since $\varepsilon > 0$), hence:

$$|\text{ND}_{ij}| = \left| \frac{b_i - b_j}{b_i + b_j + \varepsilon} \right| \leq \frac{b_i + b_j}{b_i + b_j + \varepsilon} < 1$$

Thus $\text{ND}_{ij} \in (-1, 1)$ (open interval) for all non-negative reflectance values.

(ii) For any $\mathbf{b} \in \mathcal{D}$, the vector $(\text{ND}_{ij}(\mathbf{b}))_{(i,j) \in \mathcal{N}}$ lies in the open set $(-1, 1)^{|\mathcal{N}|}$. As a polynomial, p extends continuously to the closure $[-1, 1]^{|\mathcal{N}|}$, which is compact. By continuity, $|p|$ attains its maximum M on this compact set. Since $(-1, 1)^{|\mathcal{N}|} \subseteq [-1, 1]^{|\mathcal{N}|}$, we have $|p(\mathbf{b})| \leq M$ for all $\mathbf{b} \in \mathcal{D}$.

(iii) Follows immediately: $|\tilde{p}(\mathbf{b})| = |p(\mathbf{b})|/M \leq 1$, hence $\tilde{p}(\mathbf{b}) \in [-1, 1]$. \square

This proposition has practical implications for classifier design. Given a linear classifier $f(\mathbf{b}) = w_0 + \sum_k w_k \phi_k(\mathbf{b})$ where each $\phi_k \in \Phi$, we can compute the maximum absolute value:

$$(1.9) \quad M = \max_{(\text{ND}_{ij}) \in [-1, 1]^{|\mathcal{N}|}} |f|$$

over the closed hypercube of all possible normalized difference configurations. The classifier output can then be scaled to a confidence score in $[-1, 1]$ via:

$$(1.10) \quad s(\mathbf{b}) = \frac{f(\mathbf{b})}{M}$$

This scaling leaves the decision boundary where it was, at $f(\mathbf{b}) = 0$ (and also $s(\mathbf{b}) = 0$), and simply stretches the classifier scores into a symmetric range, so values near -1 indicate high confidence in the negative class and values near $+1$ indicate high confidence in the positive class.

Our goal is to find a small subset $\mathcal{S} \subseteq \Phi$ such that a linear classifier that uses only features in \mathcal{S} still reaches high classification accuracy. Models built in this way remain easy to interpret and can be used in practice on a variety of remote sensing platforms.

Using products of normalized differences rather than single ratios has a practical benefit. When two normalized differences are multiplied, confounding effects that show up in both terms, such as changes in solar illumination or atmospheric haze, tend to cancel out, while spectral patterns that are specific to the vegetation class get amplified. This helps bring out discriminative structure that single band ratios might miss, which makes product terms useful for telling apart vegetation types that have only subtle spectral differences.

We employ three complementary feature selection algorithms, each offering distinct mechanisms for balancing classification performance against model complexity.

1.0.1. Method 1: SelectKBest with ANOVA F-Statistic. SelectKBest is a filter method that ranks features one by one according to their univariate relationship with the target variable [7]. For binary classification, the ANOVA F statistic compares the variance between classes to the variance within classes, providing a simple score for each feature.

$$(1.11) \quad F_j = \frac{\sum_{c \in \{0,1\}} n_c (\bar{\phi}_{j,c} - \bar{\phi}_j)^2}{\sum_{c \in \{0,1\}} \sum_{i: y_i=c} (\phi_{j,i} - \bar{\phi}_{j,c})^2 / (N-2)}$$

where n_c is the number of samples in class c , $\bar{\phi}_{j,c}$ is the mean of feature j in class c , and $\bar{\phi}_j$ is the overall mean. Features are ranked by F_j in descending order, and the top k features are selected.

Algorithm 1 SelectKBest Feature Selection

Require: Feature matrix $\mathbf{X} \in \mathbb{R}^{N \times |\Phi|}$, labels $\mathbf{y} \in \{0, 1\}^N$, target count k **Ensure:** Selected feature indices \mathcal{S}

- 1: **for** each feature $\phi_j \in \Phi$ **do**
- 2: Compute F-statistic F_j using ANOVA
- 3: **end for**
- 4: Rank features by F_j in descending order
- 5: $\mathcal{S} \leftarrow$ indices of top k features
- 6: **return** \mathcal{S}

1.0.2. *Method 2: Recursive Feature Elimination (RFE).* Recursive Feature Elimination is a wrapper method that iteratively removes the least important features based on a base estimator's learned coefficients [8]. Using a linear support vector machine (SVM) as the base estimator, feature importance is measured by the absolute value of the coefficient $|w_j|$.

Algorithm 2 Recursive Feature Elimination

Require: Feature matrix \mathbf{X} , labels \mathbf{y} , target count k **Ensure:** Selected feature indices \mathcal{S}

- 1: $\mathcal{S} \leftarrow \{1, 2, \dots, |\Phi|\}$ {Initialize with all features}
- 2: **while** $|\mathcal{S}| > k$ **do**
- 3: Train linear SVM on features \mathcal{S} : $f(\mathbf{x}) = \sum_{j \in \mathcal{S}} w_j \phi_j(\mathbf{x}) + b$
- 4: $j^* \leftarrow \arg \min_{j \in \mathcal{S}} |w_j|$ {Least important feature}
- 5: $\mathcal{S} \leftarrow \mathcal{S} \setminus \{j^*\}$
- 6: **end while**
- 7: **return** \mathcal{S}

1.0.3. *Method 3: L1-Regularized SVM.* L1 regularization provides an embedded feature selection approach by inducing sparsity directly through the optimization objective [30]. The L1-regularized SVM solves:

$$(1.12) \quad \min_{\mathbf{w}, b} \|\mathbf{w}\|_1 + C \sum_{i=1}^N \max(0, 1 - y_i(\mathbf{w}^T \mathbf{x}_i + b))$$

where $\|\mathbf{w}\|_1 = \sum_j |w_j|$ promotes sparsity and C controls the regularization strength. The selected features are those with nonzero coefficients: $\mathcal{S} = \{j : |w_j| > 0\}$.

For a selected feature subset \mathcal{S} with $|\mathcal{S}| = k$, we train a linear SVM to find the optimal separating hyperplane. The decision function is:

$$(1.13) \quad f(\mathbf{b}) = w_0 + \sum_{j \in \mathcal{S}} w_j \phi_j(\mathbf{b})$$

with classification rule:

$$(1.14) \quad \hat{y} = \begin{cases} +1 & \text{if } f(\mathbf{b}) > 0 \\ -1 & \text{if } f(\mathbf{b}) \leq 0 \end{cases}$$

The SVM optimization problem (with L2 regularization) is:

$$(1.15) \quad \min_{\mathbf{w}, b, \xi} \frac{1}{2} \|\mathbf{w}\|_2^2 + C \sum_{i=1}^N \xi_i$$

subject to $y_i(w_0 + \mathbf{w}^T \phi(\mathbf{b}_i)) \geq 1 - \xi_i$ and $\xi_i \geq 0$ for all i . During training, features are standardized for numerical stability:

$$(1.16) \quad \tilde{\phi}_j = \frac{\phi_j - \mu_j}{\sigma_j}$$

where μ_j and σ_j are the mean and standard deviation computed from the training set. The trained SVM produces coefficients w_j operating on standardized features. For deployment without explicit standardization, we absorb the transformation into the coefficients:

$$(1.17) \quad f(\mathbf{b}) = w_0 + \sum_{j \in \mathcal{S}} w_j \left(\frac{\phi_j(\mathbf{b}) - \mu_j}{\sigma_j} \right)$$

$$(1.18) \quad = \underbrace{\left(w_0 - \sum_{j \in \mathcal{S}} \frac{w_j \mu_j}{\sigma_j} \right)}_{\tilde{w}_0} + \sum_{j \in \mathcal{S}} \underbrace{\frac{w_j}{\sigma_j}}_{\tilde{w}_j} \phi_j(\mathbf{b})$$

The final coefficients $\tilde{w}_0, \tilde{w}_1, \dots, \tilde{w}_k$ operate directly on raw normalized difference features, enabling straightforward implementation in platforms such as Google Earth Engine without requiring access to training set statistics.

To determine the optimal number of features, we conduct a systematic sweep over feature counts $k = 1, 2, \dots, k_{\max}$:

The “sweet spot” is identified as the smallest k beyond which marginal accuracy improvements fall below a threshold ϵ (e.g., $\epsilon = 0.005$), indicating diminishing returns from additional features.

2. APPLICATION: KOCHIA DETECTION WITH SENTINEL-2 IMAGERY

Kochia (*Bassia scoparia*), often called summer cypress, is an annual broad leaf weed that has become a major issue for agriculture across the Great Plains of North America [15]. It was first brought in as an ornamental plant but has since turned into one of the most troublesome weeds in dryland cropping systems, helped by its fast growth, very high seed production (often more than 100,000 seeds on a single plant), and a tumbling way of moving that lets whole plants roll and spread seed over long distances [6]. The rise of herbicide resistant biotypes, with populations that no longer respond well to glyphosate, ALS inhibitors, or synthetic auxins, has made control even more difficult [15].

Algorithm 3 Optimal Feature Count Selection

Require: Training data $(\mathbf{X}_{\text{train}}, \mathbf{y}_{\text{train}})$, test data $(\mathbf{X}_{\text{test}}, \mathbf{y}_{\text{test}})$, maximum features k_{\max}
Ensure: Optimal feature count k^* and feature set \mathcal{S}^*

```

1: for  $k = 1$  to  $k_{\max}$  do
2:    $\mathcal{S}_{\text{RFE}} \leftarrow \text{RFE}(\mathbf{X}_{\text{train}}, \mathbf{y}_{\text{train}}, k)$ 
3:    $\mathcal{S}_{\text{KB}} \leftarrow \text{SelectKBest}(\mathbf{X}_{\text{train}}, \mathbf{y}_{\text{train}}, k)$ 
4:   for  $\mathcal{S} \in \{\mathcal{S}_{\text{RFE}}, \mathcal{S}_{\text{KB}}\}$  do
5:     Train SVM on  $(\mathbf{X}_{\text{train}, \mathcal{S}}, \mathbf{y}_{\text{train}})$ 
6:     Evaluate  $\text{Acc}_{\text{test}}(k, \mathcal{S})$  on test set
7:   end for
8:    $\mathcal{S}(k) \leftarrow \arg \max_{\mathcal{S}} \text{Acc}_{\text{test}}(k, \mathcal{S})$ 
9:   Record  $\text{Acc}(k) \leftarrow \text{Acc}_{\text{test}}(k, \mathcal{S}(k))$ 
10:  end for
11:  Identify diminishing returns:  $k^* \leftarrow \min\{k : \text{Acc}(k + 1) - \text{Acc}(k) < \epsilon\}$ 
12:  return  $k^*, \mathcal{S}(k^*)$ 

```

Remote detection of Kochia infestations would let growers manage fields in a more site specific way and step in earlier, cutting herbicide use while still keeping control levels high. In practice though, automated detection is difficult, because Kochia and the surrounding crop plants look very similar in both form and spectral response, especially when they are still in the early growth stages.

Multi-temporal Sentinel-2 imagery was acquired over agricultural fields in Saskatchewan, Canada for the growing seasons of 2022, 2023, and 2024. The Sentinel-2 MultiSpectral Instrument (MSI) provides 13 spectral bands spanning visible, near-infrared, and shortwave infrared wavelengths at spatial resolutions of 10–60 meters [4].

Ground truth labels came from field surveys, where we marked locations with confirmed Kochia and locations with crop vegetation. The full dataset contains $N = 2,318$ georeferenced sample points with binary labels: Kochia ($n = 1,247$, 53.8%) and Crop ($n = 1,071$, 46.2%). For index construction we used bands b_1 through b_{10} and left out the shortwave infrared bands (b_{11}, b_{12}) so that we focus on the visible and near infrared spectral regions where vegetation differences are most clearly expressed.

All experiments were conducted using `ndindex`, an open-source Python tool for automated spectral index discovery we developed.¹ The tool systematically generates normalized difference polynomial indices from input spectral bands and applies multiple feature selection methods to identify minimal index combinations achieving target classification accuracy.

The `ndindex` workflow runs in four steps:

- (1) **Index Generation:** Starting from the input bands, build the polynomial feature space Φ_n by computing all normalized differences and then all products of these terms up to degree two.

¹Available at <https://github.com/alilotfi90/ndindex>

- (2) **Dual Selection:** For each desired index count k , apply both SelectKBest (filter method) and RFE (wrapper method) in parallel.
- (3) **Model Comparison:** At every k compare the test accuracy of the two approaches and keep the one that performs better.
- (4) **Coefficient Export:** Fold the standardization step into the learned coefficients so the final index can be evaluated straight on raw reflectance values.

The dataset was split into a training set (70%, $N_{\text{train}} = 1,622$) and a test set (30%, $N_{\text{test}} = 696$) using stratified random sampling so the class balance stayed roughly the same in both. A fixed random seed was used so the split can be reproduced.

The normalized difference polynomial index space was then built as in Section 1, giving 1,080 candidate indices from the 10 spectral bands:

- 45 degree 1 indices (normalized differences)
- 45 degree 2 squared indices
- 990 degree 2 product indices

Index selection was carried out for target sizes $k = 1, 2, \dots, 10$, and for each k we kept whichever method, SelectKBest or RFE, gave the higher test set accuracy.

2.1. Numerical Results.

2.1.1. *Classification Performance.* Table 1 shows how test accuracy changes as we vary the number of spectral indices. With just one polynomial index we already reach 96.26% test accuracy, which suggests that Kochia has a very distinctive spectral signature that can be captured with a simple degree 2 polynomial in normalized differences. Adding more indices gives only small gains, with the best accuracy of 97.70% at $k = 8$, an increase of only 1.44 percentage points compared with the single index model.

Figure 1 plots test accuracy against the number of indices in the model. Across the whole range of k the curve hardly changes, and the single index model is already within 1.5% of the best accuracy. In practice this means that the first selected index captures almost all of the discriminative signal, with later indices only tightening the decision boundary a little.

2.1.2. *The Single-Index Kochia Classifier.* The most striking result is that a single degree-2 polynomial index suffices for highly accurate Kochia detection. The selected index is a product of two normalized differences:

$$(2.1) \quad \phi_1(\mathbf{b}) = \text{ND}_{b_4, b_5} \times \text{ND}_{b_7, b_8} = \frac{b_4 - b_5}{b_4 + b_5 + \varepsilon} \times \frac{b_7 - b_8}{b_7 + b_8 + \varepsilon}$$

where b_4 is the red band (665 nm), b_5 is red-edge 1 (705 nm), b_7 is red-edge 3 (783 nm), and b_8 is the near-infrared band (842 nm). The resulting classifier takes the form:

$$(2.2) \quad f(\mathbf{b}) = -3.7581 + 586.97 \cdot \phi_1(\mathbf{b})$$

with decision rule: classify as Kochia if $f(\mathbf{b}) > 0$, otherwise classify as Crop.

This index is mainly sensitive to how two key spectral regions behave together. The first is the red to red edge transition (b_4/b_5), where variation is driven by chlorophyll absorption, and

TABLE 1. Classification accuracy versus number of spectral indices for Kochia detection. The selection method achieving higher test accuracy is reported for each k .

k	Method	Train Acc.	Test Acc.	Gap
1	SelectKBest	0.9760	0.9626	0.0133
2	SelectKBest	0.9784	0.9655	0.0129
3	SelectKBest	0.9766	0.9641	0.0125
4	SelectKBest	0.9766	0.9655	0.0111
5	SelectKBest	0.9778	0.9698	0.0080
6	SelectKBest	0.9778	0.9698	0.0080
7	RFE	0.9895	0.9756	0.0139
8	RFE	0.9901	0.9770	0.0131
9	RFE	0.9895	0.9770	0.0125
10	RFE	0.9889	0.9770	0.0119

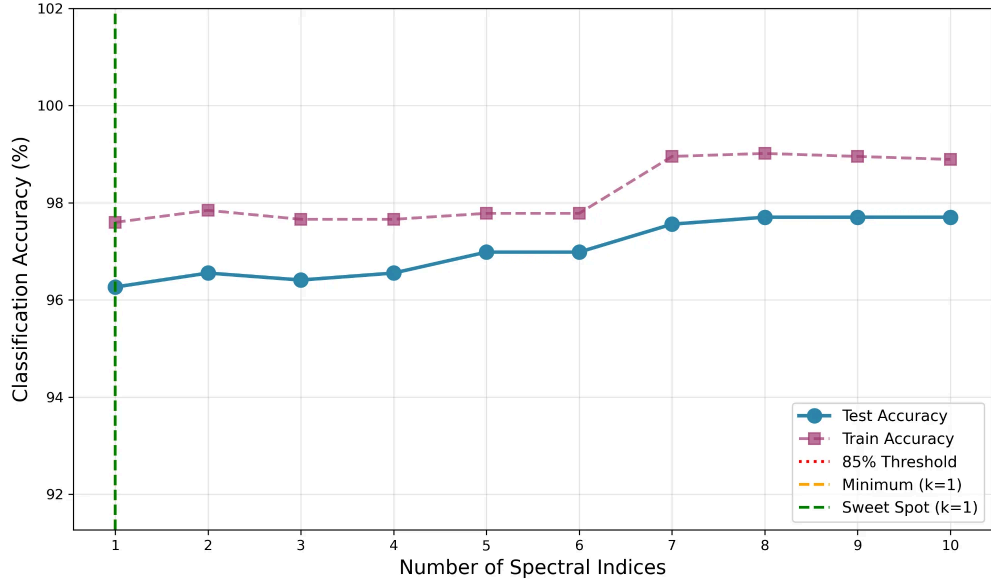


FIGURE 1. Classification accuracy as a function of the number of spectral indices. The single-index model ($k = 1$) achieves 96.26% test accuracy, with diminishing returns for additional indices. The dashed red line indicates the 85% threshold; all models substantially exceed this baseline.

the second is the red edge to NIR transition (b_7/b_8), which reflects properties of the leaf cellular structure. Taking the product of these terms highlights pixels where both transitions at once show the pattern that is characteristic of Kochia.

Table 2 presents the coefficients for models with $k = 1$ through $k = 4$ indices.

TABLE 2. Spectral indices and SVM coefficients for Kochia classifiers with $k = 1$ to $k = 4$. Coefficients incorporate absorbed standardization for direct application to raw reflectance values.

k	Term	Coefficient
1	Intercept	-3.7581
	$ND_{b_4,b_5} \times ND_{b_7,b_8}$	+586.97
2	Intercept	-4.5065
	$ND_{b_4,b_5} \times ND_{b_7,b_8}$	+250.31
	$ND_{b_4,b_6} \times ND_{b_7,b_8}$	+341.12
3	Intercept	-4.3402
	$ND_{b_4,b_5} \times ND_{b_6,b_8}$	+49.72
	$ND_{b_4,b_5} \times ND_{b_7,b_8}$	+238.35
	$ND_{b_4,b_6} \times ND_{b_7,b_8}$	+273.36
4	Intercept	-4.3821
	$ND_{b_4,b_5} \times ND_{b_6,b_8}$	+48.93
	$ND_{b_4,b_5} \times ND_{b_7,b_8}$	+247.11
	$ND_{b_4,b_6} \times ND_{b_7,b_8}$	+254.92
	$ND_{b_4,b_7} \times ND_{b_7,b_8}$	+16.24

Across all fitted models we keep seeing the same thing: every chosen index is a degree 2 product built from bands b_4 through b_8 , the red and red edge region. No degree 1 terms or simple squared terms show up in the best sets, which hints that these multiplicative combinations of normalized differences do a better job of separating classes than any single index or its square.

To quantify the benefit of degree-2 terms, we compared single-feature classifiers using degree-1 versus degree-2 features across multiple validation strategies (Table 3).

Degree-2 features outperformed degree-1 in 16 of 25 folds, confirming that the discriminative signal lies in spectral interactions rather than individual band ratios.

2.1.3. Spectral Separability. Figure 2 plots Kochia and Crop samples in the two dimensional space defined by the two most discriminative indices. The two clouds of points sit almost on separate lines with only a little overlap, which makes it easy for a basic linear classifier to reach high accuracy. Figure 3 plots the decision boundaries for models with $k = 1, 2, 3, 4$ indices, all shown in the space of the top two features. The boundaries look almost the same for every value of k , which suggests that the first index already captures nearly all of the useful separation between the classes.

TABLE 3. Accuracy comparison between degree-1 (normalized differences only) and degree-2 (including products) features using a single-index classifier.

Validation Method	Degree 1 (%)	Degree 2 (%)	Gain
Random split	92.24	96.26	+4.02
Year-held-out (3 folds)	94.15	97.12	+2.98
Spatial block (9 folds)	94.27	97.45	+3.18
Spatio-temporal (12 folds)	95.89	97.91	+2.02
Overall (25 folds)	94.95	97.58	+2.63

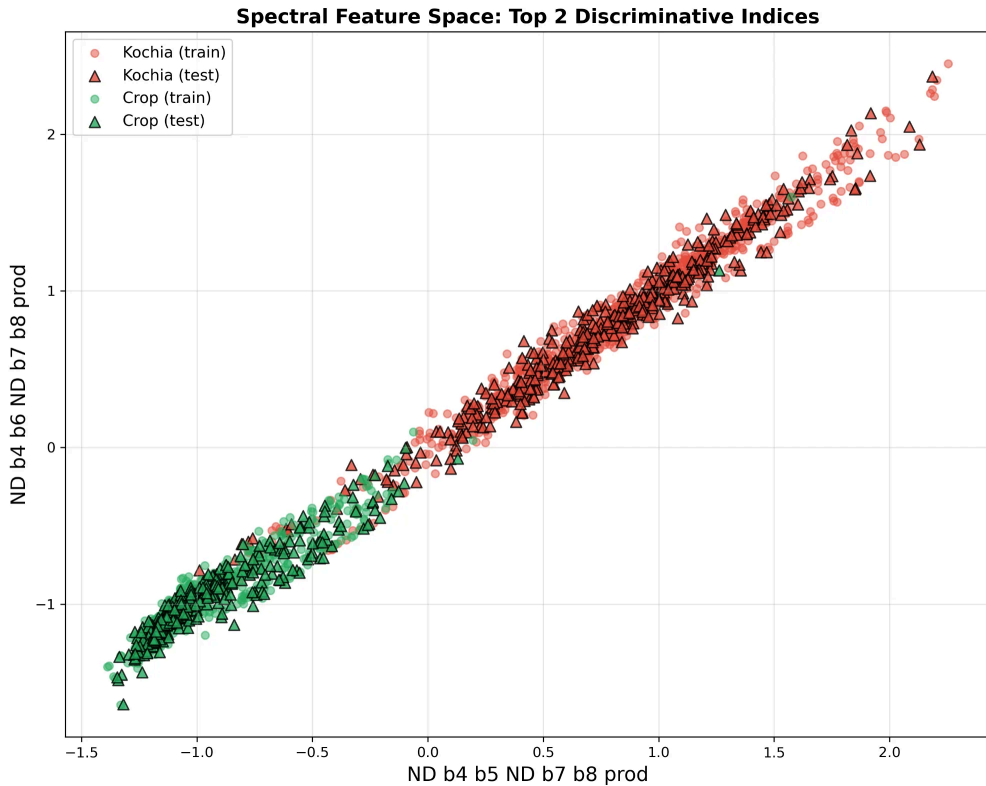


FIGURE 2. Spectral separability of Kochia and Crop samples in the feature space defined by the two most discriminative polynomial indices. The near-linear arrangement of points and clear class separation explain the effectiveness of linear SVM classification.

2.1.4. *Confusion Matrix Analysis.* Table 4 presents confusion matrices for the single-index and four-index models. The single-index model correctly classifies 315 of 322 Kochia samples (97.8%

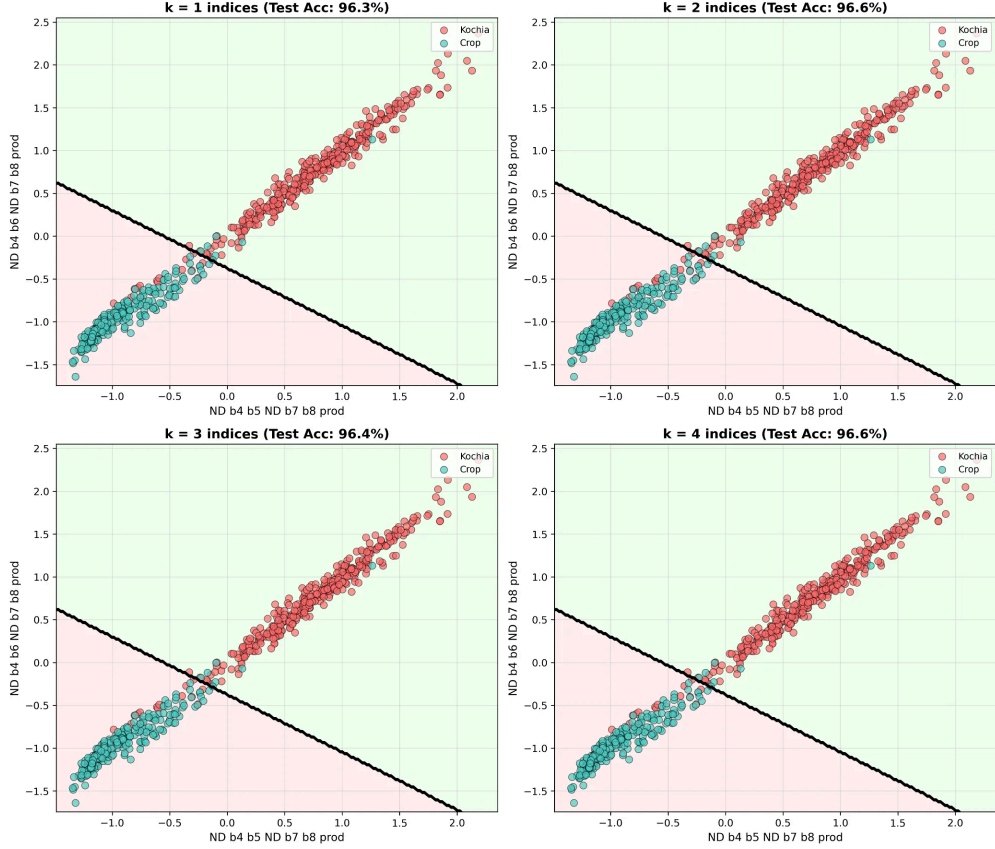


FIGURE 3. Decision boundaries for Kochia classification with $k = 1, 2, 3, 4$ spectral indices, projected onto the two most discriminative features. The consistency of boundaries across model complexities demonstrates that additional indices refine rather than fundamentally alter the classification geometry.

recall) and 355 of 374 Crop samples (94.9% specificity), with only 26 total misclassifications out of 696 test samples.

In the single index model, Kochia detection reaches a precision of 94.3% (315/334) and a recall of 97.8% (315/322), giving an F1 score of 0.960. When we move to the four index model, precision increases a bit to 94.9% (315/332) while recall stays the same, so the extra indices mostly help by cutting down false positives rather than catching more missed Kochia pixels.

2.1.5. Generalization Analysis. Figure 4 presents the train-test accuracy gap as a function of model complexity. All models maintain gaps below 1.4%, well under the 2% threshold typically indicating healthy generalization. Notably, the gap does not increase monotonically with model complexity, suggesting that the feature selection process effectively identifies genuinely discriminative indices rather than fitting to noise.

TABLE 4. Confusion matrices for the 1-index and 4-index Kochia classifiers on the test set ($N_{\text{test}} = 696$).

		Predicted	
		Kochia	Crop
		1-Index Model (Accuracy: 96.26%)	
Actual	Kochia	315	7
	Crop	19	355
		4-Index Model (Accuracy: 96.55%)	
Actual	Kochia	315	7
	Crop	17	357

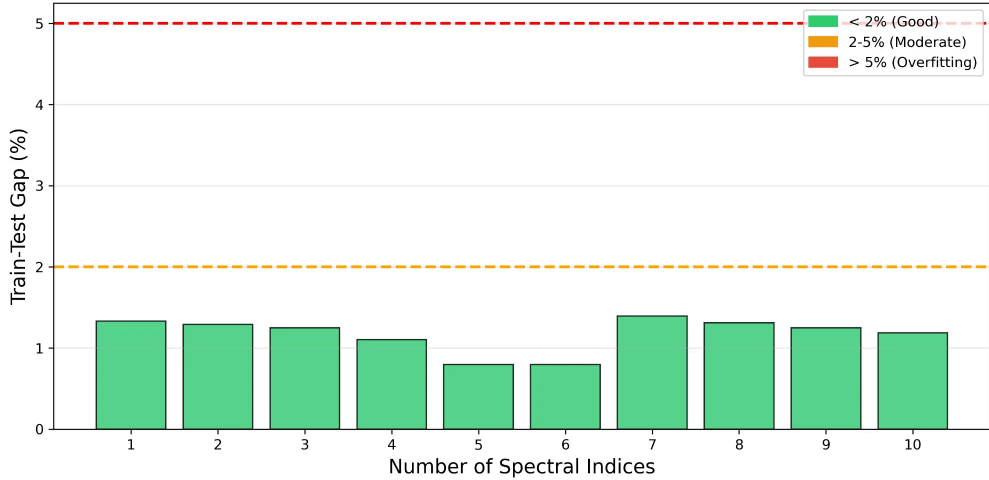


FIGURE 4. Train-test accuracy gap versus number of spectral indices. All models exhibit gaps below 2% (green zone), indicating robust generalization without overfitting. The minimum gap occurs at $k = 5$ and $k = 6$ (0.80%).

2.1.6. *Diminishing Returns Analysis.* Figure 5 shows the marginal accuracy improvement per additional index. The first index provides the baseline accuracy of 96.26%. Subsequent additions yield improvements ranging from -0.14% to $+0.57\%$, with no single addition exceeding 0.6 percentage points. Only the transition from $k = 6$ to $k = 7$ exceeds the 0.5% threshold typically used to identify meaningful improvements.

2.2. **Discussion.** While the numerical results presented here are specific to Kochia detection, the framework itself could be applied to other tasks. The polynomial embedding captures spectral interactions relevant to any vegetation discrimination problem, and the feature selection pipeline

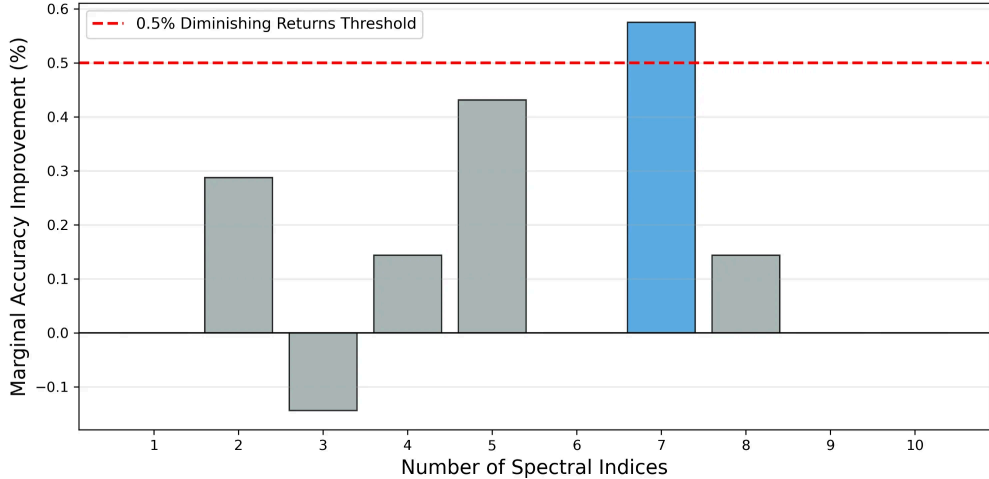


FIGURE 5. Marginal improvement in test accuracy per additional spectral index. The dashed line indicates the 0.5% diminishing returns threshold. Most improvements fall below this threshold, supporting the selection of parsimonious models.

automatically detects which interactions should be given more weight for a given task. The same workflow could be applied to crop type classification, disease detection, phenological staging, or invasive species mapping across diverse agroecosystems.

The experimental results yield several key findings with implications for both remote sensing methodology and practical weed detection: The most striking result is that a single second degree polynomial index already reaches 96.26% classification accuracy. In vegetation classification this is an unusually compact model, since studies usually rely on many features. Taken together, the result suggests that Kochia has a very distinctive spectral signature that shows up as a specific interaction within the red edge spectral regions. All selected indices across all model sizes involve bands b_4 through b_8 , spanning the red (665 nm) to NIR (842 nm) spectral region. This concentration indicates that Kochia's distinguishing spectral characteristics lie in the chlorophyll absorption edge and leaf mesophyll scattering properties, rather than in visible color differences or shortwave infrared water content signatures.

The exclusive selection of degree-2 product terms (rather than simple normalized differences or squared terms) suggests that the discriminative signal emerges from the *interaction* between spectral transitions rather than from individual band ratios. This has methodological implications: traditional single-ratio indices like NDVI may miss discriminative information encoded in cross-ratio products. The consistently low train-test gaps (< 1.4% for all models) demonstrate that the polynomial index framework avoids overfitting even when selecting from a 1,080-dimensional candidate space. The regularization provided by linear SVM combined with aggressive feature selection yields models that transfer well from training to test data.

To verify that the discovered index is not an artifact of the particular random split, we re-ran the complete feature selection procedure (searching all 1,080 polynomial features) under three alternative cross-validation strategies (Table 5). Year-held-out cross-validation—training on two years and testing on the third—achieved a mean accuracy of 97.12% ($\pm 3.79\%$). Spatial block cross-validation using a 3×3 grid (~ 4 km blocks) achieved 97.45% ($\pm 2.12\%$). Spatio-temporal blocking—holding out one year \times spatial-quadrant combination at a time—achieved 97.91% ($\pm 3.10\%$) across 12 folds. Importantly, the same index ($ND_{b_4, b_5} \times ND_{b_7, b_8}$) or its spectrally adjacent variant ($ND_{b_4, b_6} \times ND_{b_7, b_8}$, with $r = 0.996$ correlation) was selected in 24 of 25 folds (96%), confirming that the feature selection identifies a stable spectral signal rather than exploiting idiosyncrasies of the training partition. All samples originate from a single agricultural region; validation across geographically independent sites remains a direction for future work.

TABLE 5. Classification accuracy with full feature discovery repeated independently for each cross-validation fold. All 1,080 polynomial features were evaluated for each train/test partition.

Validation Method	Folds	Mean (%)	Std (%)	Min (%)
Random stratified split	1	96.26	—	—
Year-held-out	3	97.12	3.79	91.76
Spatial block (3×3)	9	97.45	2.12	92.82
Spatio-temporal block	12	97.91	3.10	90.26

The single-index classifier requires only:

- (1) Four band values: b_4, b_5, b_7, b_8
- (2) Two normalized differences
- (3) One multiplication and one linear threshold

This computational simplicity enables real-time classification in Google Earth Engine or embedded sensor systems without GPU acceleration or complex inference pipelines. Recent work by [20] reports 99.99% accuracy for Kochia detection using hyperspectral imagery with autoencoder CNN models. Our accuracy (96.26–97.70%) is lower, but the polynomial index approach brings other strengths: it is easier to interpret, since the index has a clear spectral meaning, it transfers to sensors with similar bands without needing retraining, and it is straightforward to put into practice because it is just a single arithmetic expression rather than a large deep neural network.

2.3. Corollary Embeddings. The method of generating normalized difference polynomial indices naturally yields two embeddings: one at the pixel level and the other at the vegetation-class level. Both inherit the illumination invariance and boundedness.

Definition 2.1 (Pixel-Level Embedding). For a multispectral observation $\mathbf{b} \in \mathbb{R}_{\geq 0}^n$ and polynomial degree d , we define the pixel-level embedding to be the map $\Psi_d : \mathbb{R}_{\geq 0}^n \rightarrow \mathbb{R}^{D_d}$ defined by:

$$(2.3) \quad \Psi_d(\mathbf{b}) = (\phi_1(\mathbf{b}), \phi_2(\mathbf{b}), \dots, \phi_{D_d}(\mathbf{b}))$$

where $\{\phi_1, \dots, \phi_{D_d}\}$ enumerates all monomials of degree at most d in the normalized difference basis $\{\text{ND}_{ij}\}_{i < j}$.

For each pixel, the embedding output is a fixed-length vector of polynomial feature values. The vector's dimension, denoted as D_d , depends on the number of bands n and the polynomial degree d . Specifically, with $m = \binom{n}{2}$ base normalized differences, the feature count is $D_d = \binom{m+d}{d} - 1$. For example, when $d = 2$, there are m linear terms, m squared terms, and $\binom{m}{2}$ cross-product terms. Table 6 provides embedding dimensions for commonly used sensors.

TABLE 6. Pixel-level embedding dimensions for various sensor configurations.

Sensor	Bands (n)	Base NDs (m)	D_1	D_2
Landsat OLI	7	21	21	252
Sentinel-2 (VIS-NIR)	10	45	45	1,080
Sentinel-2 (Full)	12	66	66	2,277
Hyperspectral (subset)	20	190	190	18,240

Remark. A linear classifier $f(\mathbf{b}) = w_0 + \sum_k w_k \phi_k(\mathbf{b})$ can be written as $f(\mathbf{b}) = w_0 + \langle \mathbf{w}, \Psi_d(\mathbf{b}) \rangle$.

The pixel-level embedding offers several advantages. It is illumination invariant, meaning $\Psi_d(\alpha \mathbf{b}) = \Psi_d(\mathbf{b})$ for $\alpha > 0$. The features are bounded within $(-1, 1)^{D_d}$ and interpretable, as each coordinate represents a specific spectral quantity. Additionally, this embedding can be transferred across sensors with compatible spectral bands.

The second embedding operates on vegetation classes rather than pixels.

Definition 2.2 (Class-Level Embedding). Let X be a vegetation class and \bar{X} the background. After applying feature selection and linear SVM to separate X from \bar{X} , we obtain a discriminative polynomial $f_X(\mathbf{b}) = w_0^{(X)} + \sum_k w_k^{(X)} \phi_k(\mathbf{b})$. The *class-level embedding* of X is the coefficient vector:

$$(2.4) \quad \Psi_d^{\text{class}}(X) = \left(w_0^{(X)}, w_1^{(X)}, \dots, w_{D_d}^{(X)} \right) \in \mathbb{R}^{D_d+1}$$

with unselected features set to zero.

This embedding encodes which spectral interactions distinguish a class from other cover types. Kochia, for instance, is embedded as a sparse vector with nonzero entries only for red-edge product terms. Species with similar embeddings rely on similar spectral cues; species with orthogonal embeddings are distinguished by different parts of the spectrum. One can cluster vegetation types by coefficient similarity, or track how a species' embedding shifts across regions or seasons to reveal phenological effects.

3. CONCLUSION

In this study we put together a fairly simple recipe for finding compact spectral indices using polynomial features and automatic feature selection. We start by forming all normalized differences from the multispectral bands and then build their polynomial combinations up to some fixed degree. This gives a search space that still respects the illumination invariance needed in remote sensing, but is rich enough to express nonlinear spectral patterns. On top of that space, the feature selection methods pick small sets of indices that reach the desired classification accuracy, so the final models stay readable and practical for real use.

The Kochia case study gives a few simple messages. First, a single degree two polynomial index already reaches 96.26% accuracy on its own. So some vegetation classification tasks can be handled with a very compact index, as long as the features are written in a sensible way. Second, in all of the best models the chosen indices were products of the red edge bands b_4 to b_8 . This pattern suggests that the Kochia signal comes from how chlorophyll absorption and leaf structure change together, which ordinary single ratio indices do not really capture. Third, the models hold up well when we test them, because the difference between training and test accuracy is always under 1.4% for every model size, even though the search ran over a feature space with 1,080 candidates.

The normalized difference polynomial embedding is useful beyond the particular classification task we studied here. It acts as a fixed and easy to interpret map from spectral measurements into a bounded vector space, so it gives a clear way to represent the data for many other types of analysis, such as clustering, anomaly detection, and change monitoring. In our results the learned classifiers are very sparse, usually using only one to four active dimensions. This suggests that simple low dimensional projections may already be enough for many practical applications, which can greatly reduce computing demands while still keeping the models interpretable.

In future work we see a few obvious next steps. A first step is to let the polynomial degree increase past $d > 2$, to check whether harder classification cases reveal extra structure, even if this blows up the size of the feature space. A second direction is to fold in spatial context, for instance by computing neighborhood statistics or doing simple convolution style smoothing, so the indices are less bothered by mixed pixels and sensor noise. It would also be interesting to run cross sensor transfer studies and see how well indices learned on one platform carry over to sensors with similar spectral properties. Finally, we can try the same framework on multi class classification and on regression problems, for example biomass estimation or chlorophyll content prediction, to see how far it really goes beyond binary classification.

The release of `ndindex` as open source software lets researchers run automated index discovery on their own classification problems without needing much extra programming. It helps close the gap between the clear physical meaning of classical vegetation indices and the flexibility of modern machine learning methods, so the normalized difference polynomial framework becomes a practical way to build transparent spectral classifiers that can actually be deployed in many different agricultural and environmental monitoring settings.

REFERENCES

- [1] Abdou Bannari, Daniel Morin, F Bonn, and AjRsr Huete. A review of vegetation indices. *Remote sensing reviews*, 13(1-2):95–120, 1995.
- [2] Bruno Basso and Lin Liu. Seasonal crop yield forecast: Methods, applications, and accuracies. *Advances in agronomy*, 154:201–255, 2019.
- [3] Glenn De’ath and Katharina E Fabricius. Classification and regression trees: a powerful yet simple technique for ecological data analysis. *Ecology*, 81(11):3178–3192, 2000.
- [4] Matthias Drusch, Umberto Del Bello, Sébastien Carlier, Olivier Colin, Veronica Fernandez, Ferran Gascon, Bianca Hoersch, Claudia Isola, Paolo Laberinti, Philippe Martimort, et al. Sentinel-2: Esa’s optical high-resolution mission for gmes operational services. *Remote sensing of Environment*, 120:25–36, 2012.
- [5] Dennis C Duro, Steven E Franklin, and Monique G Dubé. A comparison of pixel-based and object-based image analysis with selected machine learning algorithms for the classification of agricultural landscapes using spot-5 hrg imagery. *Remote sensing of environment*, 118:259–272, 2012.
- [6] Lyle F Friesen, Hugh J Beckie, Suzanne I Warwick, and Rene C Van Acker. The biology of canadian weeds. 138. kochia scoparia (l.) schrad. *Canadian Journal of Plant Science*, 89(1):141–167, 2009.
- [7] Isabelle Guyon and André Elisseeff. An introduction to variable and feature selection. *Journal of machine learning research*, 3(Mar):1157–1182, 2003.
- [8] Isabelle Guyon, Jason Weston, Stephen Barnhill, and Vladimir Vapnik. Gene selection for cancer classification using support vector machines. *Machine learning*, 46(1):389–422, 2002.
- [9] Driss Haboudane, John R Miller, Elizabeth Pattey, Pablo J Zarco-Tejada, and Ian B Strachan. Hyperspectral vegetation indices and novel algorithms for predicting green lai of crop canopies: Modeling and validation in the context of precision agriculture. *Remote sensing of environment*, 90(3):337–352, 2004.
- [10] Alfredo Huete, Kamel Didan, Tomoaki Miura, E Patricia Rodriguez, Xiang Gao, and Laerte G Ferreira. Overview of the radiometric and biophysical performance of the modis vegetation indices. *Remote sensing of environment*, 83(1-2):195–213, 2002.
- [11] Alfredo Huete, Christopher Justice, and Huiqing Liu. Development of vegetation and soil indices for modis-eos. *Remote Sensing of environment*, 49(3):224–234, 1994.
- [12] Alfredo R Huete. A soil-adjusted vegetation index (savi). *Remote sensing of environment*, 25(3):295–309, 1988.
- [13] Markus Immitzer, Francesco Vuolo, and Clement Atzberger. First experience with sentinel-2 data for crop and tree species classifications in central europe. *Remote sensing*, 8(3):166, 2016.
- [14] Yupeng Kang, Qingyan Meng, Miao Liu, Youfeng Zou, and Xuemiao Wang. Crop classification based on red edge features analysis of gf-6 wfv data. *Sensors*, 21(13):4328, 2021.
- [15] Vipan Kumar, Prashant Jha, Mithila Jugulam, Ramawatar Yadav, and Phillip W Stahlman. Herbicide-resistant kochia (bassia scoparia) in north america: a review. *Weed Science*,

67(1):4–15, 2019.

- [16] Gregor Laaha and Günter Blöschl. A national low flow estimation procedure for austria. *Hydrological Sciences Journal*, 52(4):625–644, 2007.
- [17] Ammarin Makkeasorn, Ni-Bin Chang, and Jiahong Li. Seasonal change detection of riparian zones with remote sensing images and genetic programming in a semi-arid watershed. *Journal of Environmental Management*, 90(2):1069–1080, 2009.
- [18] Aaron E Maxwell, Timothy A Warner, and Luis Andrés Guillén. Accuracy assessment in convolutional neural network-based deep learning remote sensing studies—part 1: Literature review. *Remote Sensing*, 13(13):2450, 2021.
- [19] Amy McGovern, Ryan Lagerquist, David John Gagne, G Eli Jergensen, Kimberly L Elmore, Cameron R Homeyer, and Travis Smith. Making the black box more transparent: Understanding the physical implications of machine learning. *Bulletin of the American Meteorological Society*, 100(11):2175–2199, 2019.
- [20] Bright Mensah, Kelvin Betitame, Joseph Mettler, Kirk Howatt, William Aderholdt, Mohamed Khan, Thomas Peters, and Xin Sun. Detection of kochia [bassia scoparia (l.) aj scott] and waterhemp [amaranthus tuberculatus (moq.) jd sauer] in sugarbeet field using hyperspectral imaging and deep learning technologies. *Pest Management Science*, 2025.
- [21] David Montero, César Aybar, Miguel D Mahecha, Francesco Martinuzzi, Maximilian Söchting, and Sebastian Wieneke. A standardized catalogue of spectral indices to advance the use of remote sensing in earth system research. *Scientific Data*, 10(1):197, 2023.
- [22] BT Mudereri, T Dube, EM Adel-Rahman, S Niassy, E Kimathi, Z Khan, and T Landmann. A comparative analysis of planetscope and sentinel sentinel-2 space-borne sensors in mapping striga weed using guided regularised random forest classification ensemble. *The International Archives of the Photogrammetry, Remote Sensing and Spatial Information Sciences*, 42:701–708, 2019.
- [23] W James Murdoch, Chandan Singh, Karl Kumbier, Reza Abbasi-Asl, and Bin Yu. Definitions, methods, and applications in interpretable machine learning. *Proceedings of the National Academy of Sciences*, 116(44):22071–22080, 2019.
- [24] Paul W Nugent, Joseph A Shaw, Prashant Jha, Bryan Scherrer, Andrew Donelick, and Vipan Kumar. Discrimination of herbicide-resistant kochia with hyperspectral imaging. *Journal of Applied Remote Sensing*, 12(1):016037–016037, 2018.
- [25] Markus Reichstein, Gustau Camps-Valls, Bjorn Stevens, Martin Jung, Joachim Denzler, Nuno Carvalhais, and F Prabhat. Deep learning and process understanding for data-driven earth system science. *Nature*, 566(7743):195–204, 2019.
- [26] Iqbal H Sarker. Deep learning: a comprehensive overview on techniques, taxonomy, applications and research directions. *SN computer science*, 2(6):1–20, 2021.
- [27] Bryan Scherrer, John Sheppard, Prashant Jha, and Joseph A Shaw. Hyperspectral imaging and neural networks to classify herbicide-resistant weeds. *Journal of Applied Remote Sensing*, 13(4):044516–044516, 2019.

- [28] Rei Sonobe, Yuki Yamaya, Hiroshi Tani, Xiufeng Wang, Nobuyuki Kobayashi, and Kan-ichiro Mochizuki. Crop classification from sentinel-2-derived vegetation indices using ensemble learning. *Journal of Applied Remote Sensing*, 12(2):026019–026019, 2018.
- [29] Lina Tang and Guofan Shao. Drone remote sensing for forestry research and practices. *Journal of forestry research*, 26(4):791–797, 2015.
- [30] Robert Tibshirani. Regression shrinkage and selection via the lasso. *Journal of the Royal Statistical Society Series B: Statistical Methodology*, 58(1):267–288, 1996.
- [31] Kate Tiedeman, Jordan Chamberlin, Frédéric Kosmowski, Hailemariam Ayalew, Tesfaye Sida, and Robert J Hijmans. Field data collection methods strongly affect satellite-based crop yield estimation. *Remote Sensing*, 14(9):1995, 2022.
- [32] Compton J Tucker. Red and photographic infrared linear combinations for monitoring vegetation. *Remote sensing of Environment*, 8(2):127–150, 1979.
- [33] Tanya S Unger Holtz. Introductory digital image processing: A remote sensing perspective, 2007.
- [34] Jinru Xue and Baofeng Su. Significant remote sensing vegetation indices: A review of developments and applications. *Journal of sensors*, 2017(1):1353691, 2017.